International Journal of Heat and Mass Transfer 131 (2019) 1270–1278

Contents lists available at ScienceDirect

International Journal of Heat and Mass Transfer

journal homepage: www.elsevier.com/locate/ijhmt

Influence of substrate temperature on Marangoni convection instabilities in a sessile droplet evaporating at constant contact line mode

Tian-Shi Wang [a], Wan-Yuan Shi [a,b,*]

[a] School of Energy and Power Engineering, Chongqing University, Chongqing 400044, China
[b] Key Laboratory of Low-grade Energy Utilization Technologies and Systems, Ministry of Education, Chongqing 400044, China

ARTICLE INFO

Article history:
Received 15 July 2018
Received in revised form 28 November 2018
Accepted 29 November 2018
Available online 4 December 2018

Keywords:
Bénard-Marangoni convection
Hydrothermal wave
Sessile droplet
Evaporation
Constant contact line mode

ABSTRACT

Marangoni instabilities of a sessile droplet of 0.65 cSt silicone oil evaporating at constant contact line mode are experimentally investigated in a wide range of the substrate temperatures (T_w) from those lower than room temperature (T_a) to those higher than it. For $T_w > T_a$, the Bénard-Marangoni convection cells are observed and the cell patterns vary from the quasi-steady state to irregular oscillatory state with the droplet evaporation. For $T_w < T_a$, the irregular oscillatory Bénard-Marangoni cells are observed when T_w is higher than 10.6 °C. The cell size is larger while there are less cell numbers compared to that of $T_w > T_a$. When T_w is higher than 14.3 °C three kinds of convection mode, i.e. the travelling hydrothermal waves, the coexistence of hydrothermal waves and irregular oscillatory Bénard-Marangoni convection, and the irregular oscillatory Bénard-Marangoni convection, occur successively with droplet evaporating. The critical contact angles for the incipience of these Marangoni instabilities are determined.

1. Introduction

Evaporation of a sessile droplet is a common phenomenon in daily life and in a wide range of scientific and industrial applications such as spray cooling [1], inkjet printing [2], DNA chips [3] and microfluidic devices [4]. Due to the nonuniform evaporation at the liquid-gas surface and different length of the thermal path, a temperature gradient is induced and the Marangoni convection would occur inside some of droplets, such as methanol, ethanol and FC-72 [5,6]. If the temperature gradient is large enough, the Marangoni convection would lose stability and instability patterns, such as hydrothermal waves (HTWs) and thermally driven cells would appear, which were observed in sessile ethanol and FC-72 droplets by Sefiane and coworkers [6]. The observed patterns in ethanol and methanol droplet resembled a wave train of alternating warm and cool regions and they traveled in the azimuthal direction. Besides, the wave number decreases linearly with time and the number of waves in the evaporating methanol drop is larger than that of the ethanol drop. It was also found that the thermal conductivity of the substrate has a significant influence on the wave number. Thus linear stability analysis as well as energy budget analysis [7,8] were adopted to study the mechanism of these waves and the results indicated the mechanism is similar to that of HTWs. Furthermore, Sefiane et al. [9] investigated the distribution of temperature and heat flux at the liquid-surface interface of an evaporating FC-72 droplet. Their results suggested that hydrothermal waves as well as thermal patterns were bulk waves which extended the whole droplet. They also found that the HTWs can influence both the solid surface temperature and the solid heat-transfer distribution. Brutin et al. [10,11] carried out a series of experiments using parabolic flight to investigate the HTWs in an evaporating ethanol droplet on a heated substrate under microgravity conditions. They found that the behaviors of these waves under microgravity were similar with those under normal gravity and the number follows a similar power law decay in an evaporating droplet with decreasing height. Thus they confirmed that it was the thermocapillary force that drove the HTWs. Stable HTWs in a sessile ethanol droplet under the steady evaporation state were investigated by Zhong and Duan [12]. They found that HTWs can be continuously maintained in a steady evaporating droplet. Moreover, the stable number of HTWs increases linearly with the increase of dimensionless factor which incorporates the normalized temperature difference between the substrate and the surroundings and the droplet aspect ratio. They also found that HTWs propagated in a manner of "one source-to- one sink" and this propagation would be weakened at a higher substrate temperature due to the appearance of new sources and sinks.

* Corresponding author.
E-mail address: shiwy@cqu.edu.cn (W.-Y. Shi).

https://doi.org/10.1016/j.ijheatmasstransfer.2018.11.155
0017-9310/

Nomenclature

a	thermal diffusivity, $m^2\ s^{-1}$
c_p	specific heat capacity, $J\ kg^{-1}\ K^{-1}$
d_{cell}	averaged thickness of cell, mm
H	droplet height, m
T	temperature, °C
ΔT	temperature difference between substrate and ambient, $\Delta T = T_w - T_a$, °C
$\Delta T'$	temperature difference between substrate and droplet apex, $\Delta T' = T_w - T_s$, °C
ΔT^*	temperature difference between droplet bottom and apex, °C
k	ratio of the tangential Marangoni number to the normal Marangoni number, $k = Ma_{//}/Ma_{\perp}$
Ma	Marangoni number with respect to ΔT, $Ma = \lvert\gamma_T\rvert\Delta TR/\mu a$
$Ma_{//}$	Marangoni number with respect to tangential temperature gradient, $Ma_{//} = \lvert\gamma_T\rvert(\partial T/\partial r)R^2/\mu a$
$Ma_{\perp}$	Marangoni number with respect to normal temperature gradient, $Ma_{\perp} = \lvert\gamma_T\rvert\Delta T'H/\mu a$
Ma^*	Marangoni number with respect to evaporation rate, $Ma^* = (\lvert\gamma_T\rvert\Delta T^*H/\mu a) + (\lvert\gamma_T\rvert V'\Delta h_v H^2/\mu c_p a^2)$
Bo_d	dynamic Bond number, $Bo_d = \rho g\beta H^2/\gamma_T$
R	wetting radius of droplet, m
t	evaporating time, s
λ_{cell}	wave length of cell, mm
Δh_v	latent heat of vaporization, $J\ kg^{-1}$
V'	volumetric evaporation rate per unit area, $m^3\ m^{-2}\ s^{-1}$
z	vertical axis coordinate, m
r	radial coordinate, m

Greek symbols

ρ	density, $kg{\cdot}m^{-3}$
λ	thermal conductivity, $W\ m^{-1}\ K^{-1}$
μ	dynamic viscosity, $kg{\cdot}m^{-1}\ s^{-1}$
γ_T	temperature coefficient of surface tension, $N{\cdot}m^{-1}\ K^{-1}$
σ	surface tension, $N\ m^{-1}$
β	volumetric thermal expansion coefficient, K^{-1}
θ	contact angle, °
ε	emissivity

Subscripts

0	initial value
a	ambient
c	critical value
w	substrate
s	droplet apex value
BM	Bénard-Marangoni convection
OBM	irregular oscillatory Bénard-Marangoni convection
HTW	hydrothermal wave

It is worth to point out that both the tangential temperature gradient parallel to the free surface and the normal temperature gradient perpendicular to surface coexist inside the droplet due to the curved surface of the droplet. Furthermore, the tangential temperature gradient drives the thermocapillary convection and leads to the HTW instability while the normal temperature gradient tends to induce another Marangoni instability named Bénard-Marangoni (BM) instability. In the last more than one hundred years, plenty of works have been conducted on BM instability in flat liquid layer [13–23] whereas few of them observed it in evaporating droplet. A flow visualization using aluminum suspension was performed by Zhang and Yang [24] to investigate the flow structure in an evaporating droplet of chloroform, methylene chloride, etc., and the BM convection cells were observed in droplets. The BM instability patterns in a silicone oil droplet with low volatility on a heated substrate were numerically obtained by Shi et al. [25]. With increasing Ma number, steady BM convection and irregular oscillatory BM convection were generated respectively. Semenov et al. [26,27] proposed the one-side model and investigated the Marangoni instability in a sessile ethanol droplet on a heated substrate with a pinned contact line under weightlessness conditions by three-dimensional unsteady simulations. Their numerical results indicated that the previously observed patterns were actually unsteady BM instability rather than HTWs because the wavelength of cells is about twice the local droplet thickness. Zhu et al. [28] conducted a series of experiments as well as three-dimensional simulations to investigate the Marangoni instability in the evaporating droplet at constant contact angle mode. The quasi-steady state flower-like patterns made-up by BM cells were observed in the droplet and the cell number decreases one by one with the contact line receding, which follows a square function of the evaporating time.

Although both HTW and the BM instability may occur inside the evaporating droplet, the detailed conditions for the incipience of them are not yet clear. In present work, a series of experiments are conducted to investigate the Marangoni instabilities in a sessile droplet evaporating at constant contact line (CCL) mode. A wide range of substrate temperatures from those lower than the room temperature to those higher than it are adopted. Both HTW instability and BM instability are observed and the critical conditions for the incipience of them are determined.

2. Experimental apparatus

The experimental apparatus contains a cylindrical stainless steel substrate, a contact angle meter, an infrared camera and a thermostatic oil bath, as shown in Fig. 1. The temperature of the substrate is controlled by the thermostatic oil inside a cylindrical vessel under the substrate linked with a thermostatic oil bath (PP07R-20-A12Y from PolyScience Inc.) with temperature stability of ±0.005 °C. Four T-type thermocouples (Omega Engineering Inc.) with diameter of 0.25 mm are fixed on the substrate to measure

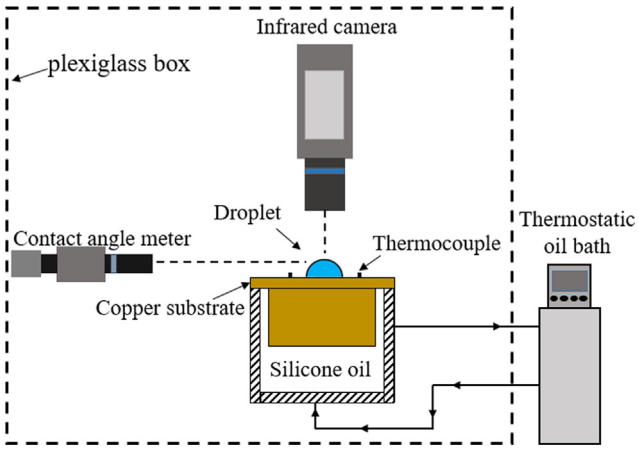

Fig. 1. Schematic of experimental apparatus.

the practical temperature of the substrate. The maximum error of the thermocouple is ±0.04 °C after calibrated by the thermostatic oil bath from 0 °C to 35 °C. The diameter of the stainless steel substrate is about 100 mm, i.e., over 20 times larger than the diameter of the droplet, to ensure the uniform temperature of droplet bottom. The surface of the substrate is mirror polished firstly and then coated with a thin layer of hydrophobic coating (FC-3120) by a micro-spray gun. The 0.65 cSt silicone oil (KF-96L, Shin-Etsu Chemical Co., Ltd) is used as the test fluid and the physical properties of the silicone oil are listed in Table 1. Where, the temperature coefficient of the surface tension is defined as $\gamma_T = -\partial\gamma/\partial T$. The initial volume of the sessile droplet is controlled at 6.0–7.5 μl in order to ensure that the droplet radius is almost constant at each substrate temperature. The sessile droplet is initially at room temperature (21.0 °C ± 0.30 °C) and it is deposited at the center area of the substrate by a micro-syringe with a manual control whose needle is placed very close (~5mm) to the substrate. The surface thermal pattern of the droplet is observed by an infrared camera (FLIR A655sc) with the thermal sensitivity less than 30 mK at 30 °C and the frequency of 50 Hz at 640 × 480 pixels. A close-up IR lens with a view field of 16 mm × 12 mm is mounted on the camera and a spatial resolution of 25 μm can be achieved. The mean penetration thickness of silicone oil for radiation with wavelength of 8–12 μm is 0.012 mm approximately and thus the temperature recorded by the IR camera is the droplet surface rather than the bulk surface [29,30]. The contact angle of the droplet is measured by a contact angle measurement (JC2000DM from Shanghai Zhongchen Digital Technic Apparatus Co., Ltd) with error of 0.1° and resolution of 0.01°. In the experiments, the droplet is well symmetrical and the contact angles on both sides are consistent with the maximum discrepancy of ±0.5°. All the data of the contact angle in this paper is the average value of the left contact angle and the right one. As shown in Fig. 2, the contact angle of the droplet decreases linearly with evaporating time until it reduces to be about 7° whereas the wetting radius almost remains unchanged, which indicates that the evaporation is constant contact line mode. It should be noted that the droplet in our experiments evaporates at constant contact radius mode until it disappears. However, the contact angle is hard to measure precisely when θ is less than 7° and this final stage maintains only about 17 s which occupies only 13 percent of the lifetime of the droplet (~130 s). Actually, the droplet is very close to a flat thin liquid layer and the Marangoni convection instability during the final stage is not what we really care about. For all the experiments, the ambient temperature is controlled at T_a = 21.0 °C with the maximum fluctuation of ±0.30 °C. To reduce the effect of the environment air flow on the evaporation, the main experiment apparatus is covered by a plexiglass box (594 mm × 718 mm × 899 mm). The maximum droplet height in the experiments is H = 0.95 mm which is less than the capillary length ($\lambda_{cp} = \sqrt{\sigma/\rho g}$ = 1.44 mm) and thus the droplet is considered to maintain a spherical cap. Additionally, the dynamic Bond number is Bo_d = 0.11 which is very small and thus the effect of buoyancy can be neglected. The experiment is repeated at least four times under each substrate temperature to ensure the repeatability of the results.

Table 1
Physical properties of 0.65 cSt silicone oil at 298.15 K.

Physical property	Value
Density, ρ	760 (kg m^{-3})
Specific heat capacity, c_p	2000 (J kg^{-1} K^{-1})
Thermal conductivity, λ	0.1 (W m^{-1} K^{-1})
Dynamic viscosity, μ	4.94×10^{-4} (kg m^{-1} s^{-1})
Surface tension, σ	1.54×10^{-2} (N m^{-1})
Volumetric thermal expansion coefficient, β	1.34×10^{-3} (K^{-1})
Surface tension temperature coefficient, γ_T	-8×10^{-5} (N m^{-1} K^{-1})
Latent heat of vaporization, Δh_v	2.23×10^{5} (J kg^{-1})
Emissivity, ε	0.91

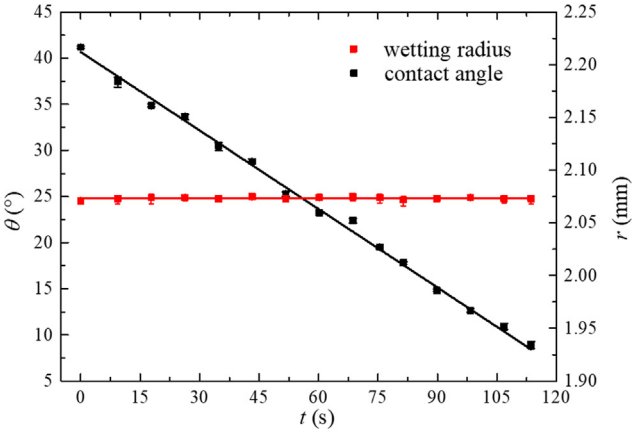

Fig. 2. The evolution of the contact angle and the wetting radius of a droplet during evaporation at T_w = 25.03 °C, T_a = 20.98 °C and the relative humidity of 66%.

3. Experimental results and discussions

The Marangoni convection patterns for those when the substrate temperature is higher than the room temperature ($T_w > T_a$) and those lower than the room temperature ($T_w < T_a$) are observed in the experiments. They will be introduced in Sections 3.1 and 3.2 respectively.

3.1. Marangoni convection patterns for $T_w > T_a$

One typical example of the Marangoni convection pattern for $T_w > T_a$ is shown in Fig. 3. Its initial contact angle is θ_0 = 40.23° and the wetting radius is R = 2.07 mm. At the early period after the droplet is deposited onto the substrate, the surface temperature is almost axisymmetric and the temperature near the contact line is higher than that of apex region (Fig. 3a). Thus the flow is steady thermocapillary convection. With the droplet evaporating, when the contact angle reduces to θ = 30.81° at t = 41.15 s, two small light cells appear near the triple-line (Fig. 3b) and each of them separates into two new cells. With time going on, more cells come out and totally sixteen cells are uniformly distributed in the droplet at t = 46.95 s and they make up a flower-like patterns (Fig. 3c). The outer profile of each cell is circular-arc and it looks like a petal. The pattern and the cell number almost remains unchanged within the next 25 s. During this period the contact angle decreases continuously and thus it is actually a quasi-steady state. When contact angle reduces to 21.85° at t = 72.11 s, another two small cells are generated near the central region (marked by 'Generated cells' in Fig. 3d). They grow up quickly and soon each of them separates into two new cells (Fig. 3e). They extend to the region near the triple-line and merges with the original cells there (Fig. 3f). After a while, another cell emerges (marked by 'Generated cell' in Fig. 3g) and it soon separates into two new cells (Fig. 3h). With droplet evaporating and its height decreasing, more and more cells are generated from the central region and they move outwards along radius direction. The original cells near the triple-line are then pushed outward and their sizes become smaller and some of them vanish eventually. Meanwhile, the region occupied by large cells decreases and they gradually concentrate in the central region. During this period after t = 72.11 s the patterns are not quasi-steady but irregular oscillatory. Similar patterns were obtained by Shi et al. [25] in their

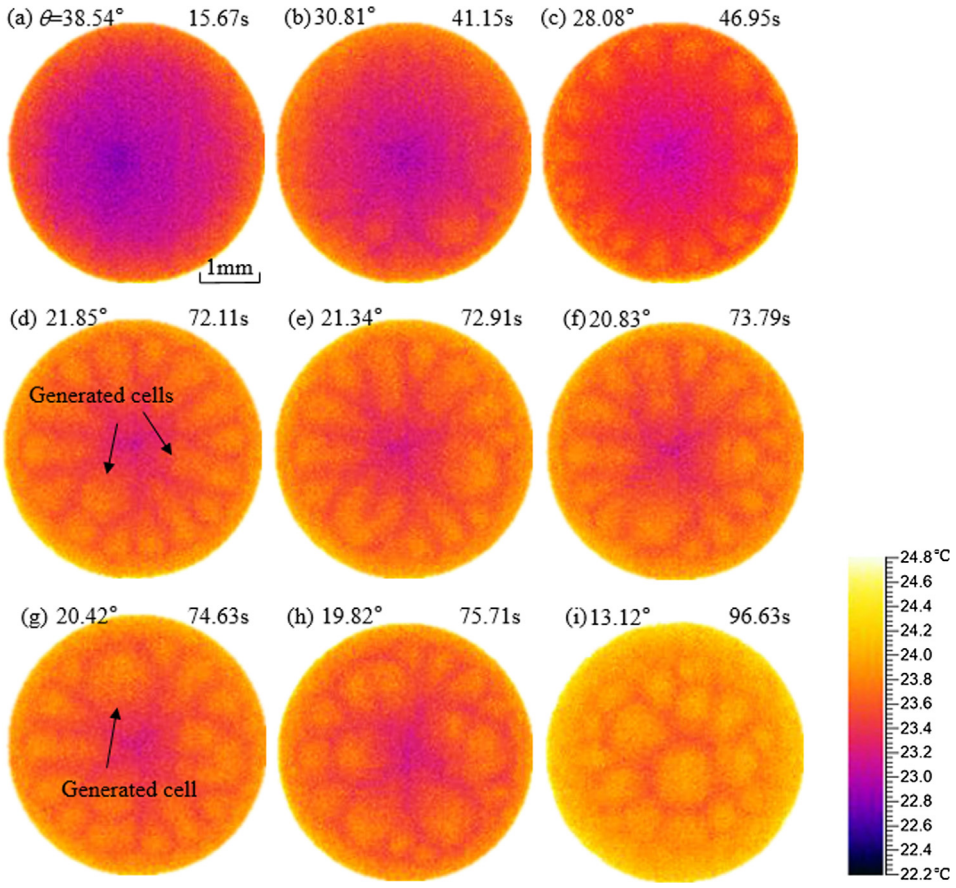

Fig. 3. Evolution of the surface temperature patterns of a droplet with the initial contact angle of $\theta_0 = 40.23°$ and the radius of $R = 2.07$ mm at $T_w = 25.13$ °C, $T_a = 21.01$ °C and the relative humidity of 61% for (a) $\theta = 38.54°$ at $t = 15.67$ s, (b) $\theta = 30.81°$ at $t = 41.15$ s, (c) $\theta = 28.08°$ at $t = 46.95$ s, (d) $\theta = 21.85°$ at $t = 72.11$ s, (e) $\theta = 21.34°$ at $t = 72.91$ s, (f) $\theta = 20.83°$ at $t = 73.79$ s, (g) $\theta = 20.42°$ at $t = 74.63$ s, (h) $\theta = 19.82°$ at $t = 75.71$ s and (i) $\theta = 13.12°$ at $t = 96.63$ s.

numerical simulations of 1 cSt silicone oil droplet although they neglected the effect of evaporation on droplet deformation. After $t = 96.63$ s the cells become polygonal (Fig. 3i) which are very similar to the classical BM convection cells found by Bénard in bottom heated flat liquid layer [13,14]. In fact, the contact angle at this moment is very small and the droplet is close to a flat thin layer. The region dominated by the cells becomes small and the cells sizes are small. These polygonal cells always exist in the droplet and their sizes become smaller and smaller with droplet evaporating. Finally, these polygonal cells vanish when the time is very close to the end of the lifetime of the droplet.

For a higher substrate temperature, for example at $T_w = 29.54$ °C, a small cell appears at the region near the triple-line which is slightly earlier comparing with that at low T_w when the contact angle is reduced to $\theta = 32.97°$ at $t = 35.01$ s (Fig. 4a). After a while eighteen cells make up a flower pattern at $t = 48.41$ s (Fig. 4b). The cell number is larger than that at low T_w in Fig. 3(c) and thus the circumferential width of the cell is smaller. Moreover, the cells are slightly longer and the region dominated by the cells is wider. The quasi-steady state maintains only about six seconds until a small cell appears near the triple-line at $t = 54.81$ s (Fig. 4c). Then this cell separates into two small cells and they merge with the original cells near the triple-line (Fig. 4d). With droplet evaporating, new cells are always generated at the central region which is similar to that of a low T_w, but the cells grow faster and the pattern becomes more irregular. Besides, many polygonal cells as those in Fig. 3(i) yields after $t = 84.92$ s (Fig. 4f). Experiment results show that the maximum cell number of the patterns under quasi-steady state (e.g. from Fig. 4b to c) increases linearly with the increase of the Marangoni number of *Ma* (by increasing the substrate temperature), as shown in Fig. 5. The *Ma* number is defined as $Ma = |\gamma_T|\Delta TR/\mu a$, where ΔT represents the temperature difference between the surface of substrate and the ambient.

Fig. 6 summarizes the ratio of wave length of the cell λ_{cell} at the quasi-steady state to its local averaged thickness d_{cell} versus Marangoni number. For the quasi-steady state, the wavelength of the cell is the width of the cell measured through the thermal image. Meanwhile, the local thickness is the droplet height where the center of the cell locates and it is measured by contact angle measurement. The local averaged thickness of the cells decrease with the droplet evaporating whereas the wave length of the cells maintain almost constant during the whole quasi-steady state. Thus the ratio of λ_{cell} to d_{cell} increases during the whole quasi-steady state with the droplet evaporating and the average value varies from 3.55 (dashed black line in Fig. 6) to 4.41 (dashed red line in Fig. 6). These values are close to that of 3.88 for the hexagon pattern observed in an evaporating flat liquid layer by Mancini and Maza [31], and that of 3.0 in bottom heated flat layer [32]. Moreover, the ratio of λ_{cell} to d_{cell} is independent of the *Ma* number when the substrate temperature varies from $T_w = 22.27$ °C to 29.64 °C. We thus believe that the cells observed in present experiments are BM cells. However, as mentioned above, the outer profile of the cell in droplet is circular-arc, which is different from that in flat layer. The reason is that only circular profile can satisfy the condition that the ratio of the wavelength to the thickness of the cells is constant in spherical-cap droplet [25] whereas the

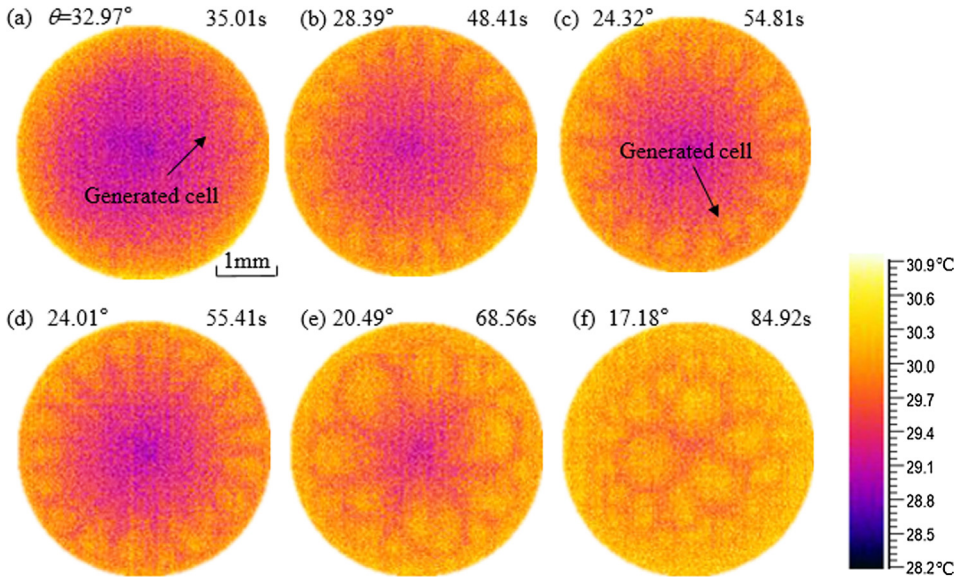

Fig. 4. Evolution of the surface temperature patterns of a droplet with the initial contact angle of $\theta_0 = 46.03°$ and the radius of $R = 2.09$ mm at $T_w = 29.54$ °C, $T_a = 21.73$ °C and the relative humidity of 60% for (a) $\theta = 32.97°$ at $t = 35.01$ s, (b) $\theta = 28.39°$ at $t = 48.41$ s, (c) $\theta = 24.32°$ at $t = 54.81$ s, (d) $\theta = 24.01°$ at $t = 55.41$ s, (e) $\theta = 20.49°$ at $t = 68.56$ s and (f) $\theta = 17.18°$ at $t = 84.92$ s.

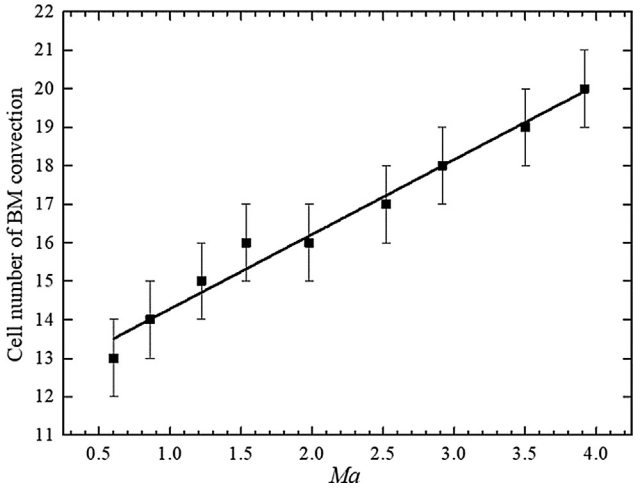

Fig. 5. The cell number of the steady BM convection versus *Ma* number. The error bar indicates the discrepancy between the maximum cell number of BM convection from the average one.

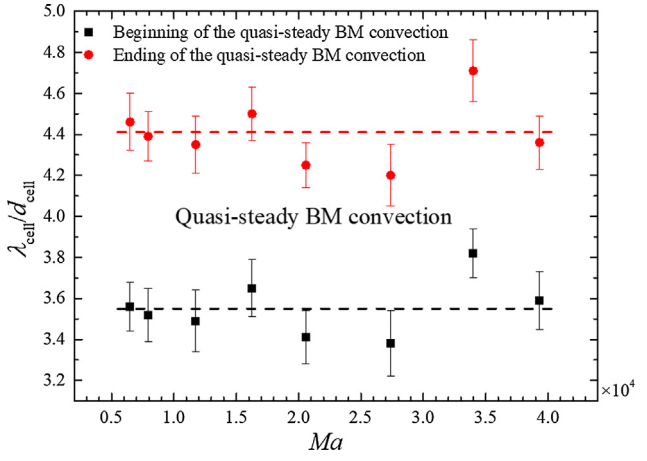

Fig. 6. The ratio of the wave length of the cell λ_{cell} to its local averaged thickness d_{cell} during the quasi-steady state versus *Ma* number. The dashed lines denote the averaged values of the dots. The error bar indicates the discrepancy between the maximum value of λ_{cell}/d_{cell} from the average one.

linked straight line between the cells are caused by the squash of the cells.

As mentioned above, both the tangential and the normal component of the temperature gradient always coexist in the droplet. Here, we define a parameter $k = Ma_{//}/Ma_{\perp}$ to represent the ratio of the tangential Marangoni force to the normal one. The $Ma_{//} = |\gamma_T|(\partial T/\partial r)R^2/\mu a$ denotes the tangential *Ma* number measured at triple-line while the $Ma_{\perp} = |\gamma_T|\Delta T' H/\mu a$ indicates the normal *Ma* number measured at the apex of the droplet. Here, $\Delta T'$ represents the temperature difference between the surface of substrate and the droplet apex. The former one is measured by thermocouples while the latter one is done by IR camera and calibrated by thermocouple. Fig. 7 shows the radial temperature distribution on droplet surface of three typical cases, i.e. steady thermocapillary convection (Fig. 3a), the onset of the steady BM convection (Fig. 3b) and the onset of the irregular oscillatory BM convection (Fig. 3d) respectively. And then the fitting curve of the radial temperature distribution is obtained and the slope of which is the corresponding value of the radial temperature gradient. As shown in Fig. 8, the value of *k* declines linearly with the decrease of contact angle during evaporation. The tangential temperature gradient at the triple-line is high when $\theta = 38.54°$ (Fig. 3a) which can be seen from the case 1 in Fig. 7 and the value of *k* is 3.88 at this time. It indicates that the flow is dominated by the tangential Marangoni force and the thermocapillary convection is preferred in the droplet at that moment. With evaporation, the normal Marangoni number decreases due to decreasing height and it is reduced to be $Ma_{\perp} = 2628.68$ when $\theta = 30.81°$ (Fig. 3b). It is still quite larger than the critical $Ma_{\perp,c}$ (=79.6 for $Bi = 0$) for the onset of BM convection in bottom heated flat liquid layer [16]. More importantly, the value of *k* is reduced to be 2.09 at this moment which indicates that both the tangential Marangoni force and the stabilization effect on BM convection become weak. Thus the BM convection occurs at this moment even though the normal Marangoni number is lower than that of Fig. 3(a). When the contact angle reduces to 21.85° (Fig. 3d) the *k* further reduces to 1.04. The normal Marangoni force becomes

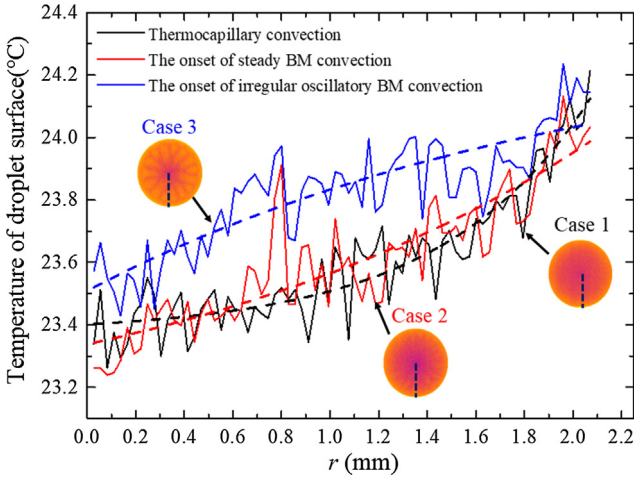

Fig. 7. Radial temperature distribution on droplet surface of three typical cases shown in Fig. 3(a), (b) and (d) respectively. The dashed line represents the fitting curve of the radial temperature distribution.

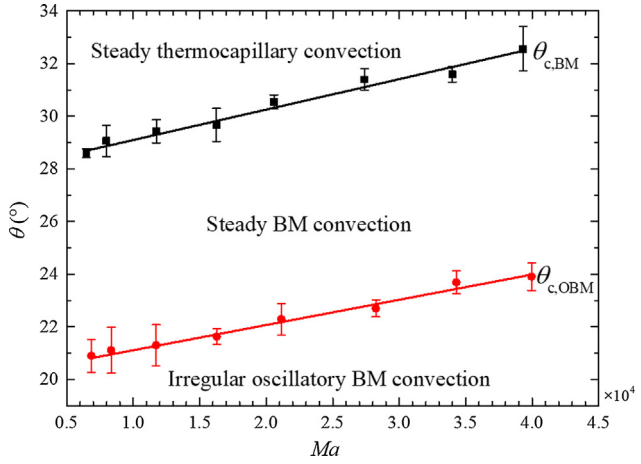

Fig. 9. The critical contact angles for incipience of the steady BM Marangoni convection and the irregular oscillatory BM convection for $T_w > T_a$. The error bar indicates the discrepancy between the maximum value of contact angle from the average one.

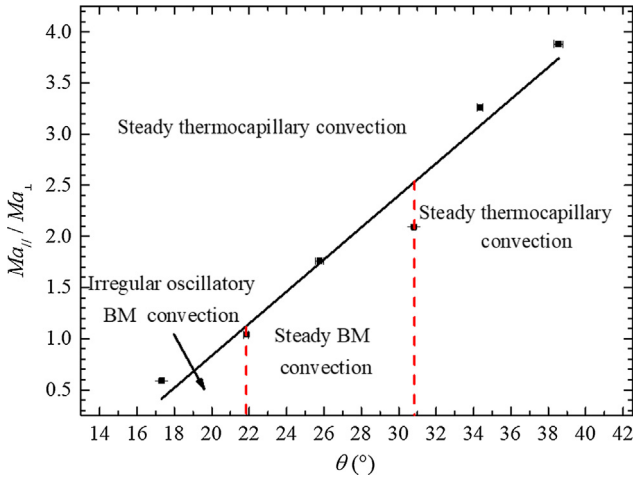

Fig. 8. The evolution of the ratio of $Ma_{//}/Ma_{\perp}$ versus the contact angle during evaporation of the droplet shown in Fig. 3.

more important and thus the irregular oscillatory patterns come out.It should be noted that cells mainly appear at the region near the triple-line when the contact angle is large (Fig. 3b and c). It is because the normal temperature gradient at the region near the triple line is larger than that of the central region due to the higher evaporation rate near the triple-line. Here, we measure the vertical temperature gradient near the triple-line and at the droplet apex when the time is close to the onset of convection cells (Fig. 3b) respectively. The value of the latter one is $\partial T/\partial z = 4.06$ °C/mm which is smaller than that of the former one $\partial T/\partial z = 5.21$ °C/mm, which verifies our idea. However, the cells mainly limit at the central region (Fig. 3i) when the evaporation is close to the end of lifetime. That is because the droplet height near the triple-line is smaller than the critical thickness for the onset of BM cells in liquid thin layer [33]. Here, we measure the height at the region with $R = 1.66$ mm where the boundary of BM cells locates in Fig. 3(i), whose value is 0.078 mm and it is smaller than the critical thickness for the onset of BM cells in liquid thin layer ($d_c = \sqrt[3]{120\mu a/\rho g} = 0.081$ mm). Thus the BM cells do not occur anymore and it is replaced by the thermocapillary convection.

Fig. 9 illustrates the critical contact angles for the incipience of the quasi-steady BM convection and the irregular oscillatory BM convection. Both of them increase linearly with increasing the *Ma* number. As mentioned above, the *Ma* number is defined as $Ma = |\gamma_T|\Delta TR/\mu a$ to highlight the influence of substrate temperature on the Marangoni instabilities, which is different from the $Ma_{\perp}$ and $Ma_{//}$ defined before, where ΔT represents the temperature difference between the surface of substrate and the ambient. It should be noted that the stabilization of the thermocapillary convection is strong because of the high tangential temperature gradient when the contact angle is large. The BM convection can only occur when the contact angle is reduced to a certain value ($\theta_{c,BM}$). For the same reason, the irregular oscillatory BM convection onsets when the contact angle is reduced to $\theta_{c,OBM}$. With increasing the *Ma* number, the normal Marangoni force perpendicular to the droplet surface becomes more and more significant and the BM convection cells would appear more easily. Thus the critical contact angle for the onset of steady BM convection increases with increasing *Ma* number and meanwhile, $\theta_{c,OBM}$ also increases with increasing *Ma* number.

3.2. Marangoni convection patterns for $T_w < T_a$

When the temperature of substrate is lower than 10.6 °C, the flow is steady thermocapillary convection during the whole lifetime of the droplet and the BM convection cells only initiate when T_w is higher than 10.6 °C. One example is shown in Fig. 10. The sizes of cells are larger while the cell number is smaller than those of $T_w > T_a$. One new small cell is generated at the central region of the droplet (marked by 'Generated cells' in Fig. 10a) and it is growing larger with droplet evaporating (Fig. 10b). Then it separated into two small cells (marked by 'Separated cells' in Fig. 10c). The cells are separating, drifting and deforming continuously which is similar with that of the irregular oscillatory BM convection when $T_w > T_a$. The distribution of the cells is not uniform and the cells are quite weak and it is difficult to distinguish because of the low T_w. When the contact angle is less than 14.95°, few cells are generated again and the cells become polygonal (Fig. 10d) as same as those in Figs. 3(i) and 4(f).

With increasing the substrate temperature, for example when $T_w = 14.5$ °C, a kind of traveling wave patterns are observed in a droplet with the initial contact angle of $\theta_0 = 34.41°$ and the wetting radius of 2.23 mm (Fig. 11a). The waves travel from a source to a sink, which are composed of the clockwise propagating waves and the counterclockwise propagating waves. It should be noted

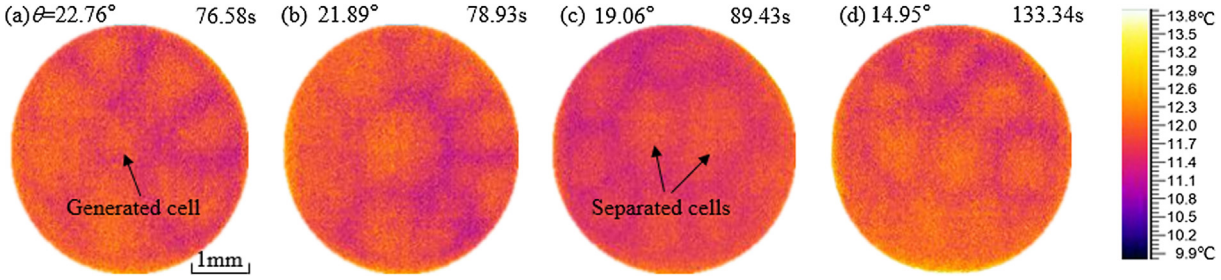

Fig. 10. Evolution of surface temperature patterns of droplet with the radius of $R = 2.16$ mm at $T_w = 12.45$ °C, $T_a = 21.89$ °C for (a) $\theta = 22.76°$ at $t = 76.58$ s, (b) $\theta = 21.89°$at $t = 78.93$ s, (c) $\theta = 19.06°$ at $t = 89.43$ s and (d) $\theta = 14.95°$ at $t = 132.23$ s.

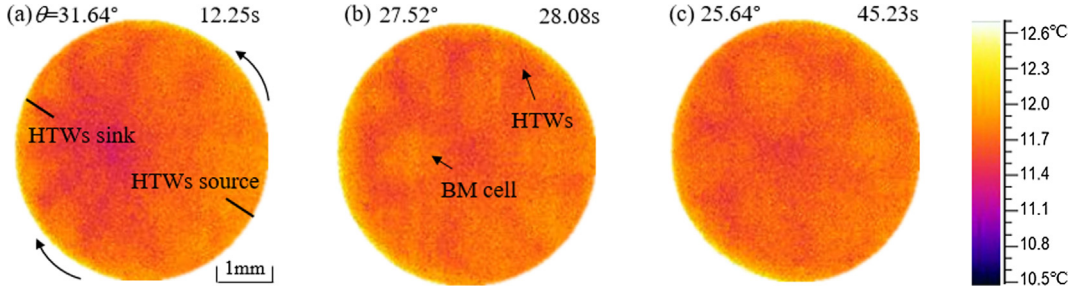

Fig. 11. Evolution of the surface temperature patterns of a droplet with the radius of $R = 2.23$ mm at $T_w = 14.50$ °C, $T_a = 21.45$ °C and the relative humidity of 47% for (a) $\theta = 31.64°$ at $t = 12.25$ s, (b) $\theta = 27.52°$ at $t = 28.08$ s and (c) $\theta = 25.64°$ at $t = 45.23$ s.

that the source and the sink always exists and their locations almost remains unchanged during the evaporation for this case, which means that these traveling waves always propagate along their fixed directions. These patterns share some common characteristics of the HTWs observed in ethanol and methanol droplets by Sefiane et al. [6] and by Sobac and Brutin [10]. We thus believe that these travelling waves are HTWs. For this case, the tangential temperature gradient at the triple-line is large which can be seen from case 1 in Fig. 12. The tangential Marangoni number is $Ma_{//} = 12376.13$ and the value of k is $k = 3.89$ at this moment which indicates that the tangential Marangoni force is quite strong and thus the strong thermocapillary convection leads to the HTWs. However, the HTWs can't maintain its state continuously due to evaporation and decreasing contact angle. At $t = 28.08$ s, the temperature gradient at the triple-line decreases (case 2 in Fig. 12) and k reduces to be 2.73. The HTWs are faded and some of them

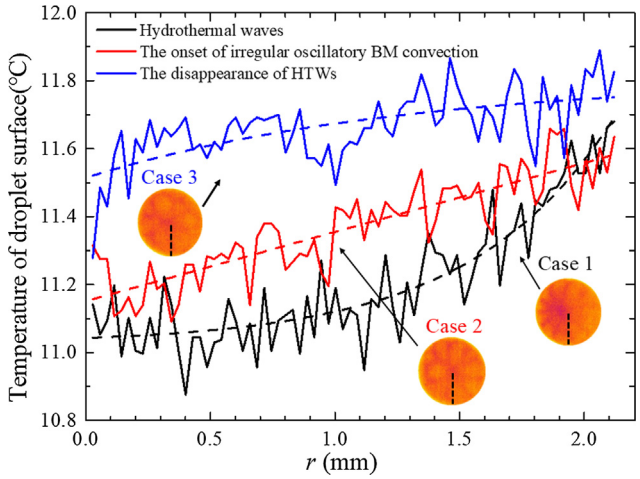

Fig. 12. Radial temperature distribution on droplet surface of three typical cases shown in Fig. 11(a), (b) and (c) respectively. The dashed line represents the fitting curve of the radial temperature distribution.

are replaced by irregular oscillatory BM cells (Fig. 11b). At $t = 45.23$ s the k reduces to be 1.26 and the HTWs are completely disappeared and only the irregular oscillatory BM cells exist inside the droplet (Fig. 11c). It is interesting that Shklyaev and Nepomnyashchy [34] obtained a similar conclusion in a flat liquid layer subjected to an inclined temperature gradient. They predicted that the BM cells would transform into the HTWs if the tangential temperature gradient is increased.

For higher substrate temperature, such as at $T_w = 18.23$ °C, a similar HTWs are observed as shown in Fig. 13(a), which also travel from a source to a sink but faster than those at lower T_w. It is worth mentioning that the locations of the source and the sink in this case are different from those in Fig. 11(a) and a series of experiment results indicate that the positions of the source and the sink are random without preferred location. We thus reasonably exclude the influences of the nonuniform substrate temperature or the perturbation of environment air flow on the positions of the source or the sink. With the droplet evaporating, the BM cells occur when $t = 40.77$ s (Fig. 13b) at a higher contact angle of $\theta = 30.92°$ than those at lower T_w. After a period, the HTWs completely vanish at $t = 64.31$ s and only the irregular oscillatory BM cells exist inside the droplet (Fig. 13c). The BM cells grows faster and their sizes are smaller than those at lower T_w.

Fig. 14 summarizes the critical contact angles for the onset of the Marangoni convection instabilities for $T_w < T_a$. Just like the Ma number in Fig. 9, the Ma number here is also defined as $Ma = |\gamma_T|\Delta TR/\mu a$, where ΔT represents the temperature difference between the surface of substrate and the ambient. The HTWs occur when $Ma > -38475.32$ ($T_w > 14.3$ °C) under a contact angle higher than the $\theta_{c,OBM}$ (black line in Fig. 14). When the contact angle is reduced to $\theta_{c,OBM}$, the irregular oscillatory BM convection appears. Under this condition, the HTWs do not fully disappear and some of them coexist with the BM cells, as shown in Figs. 11(b) and 13(b). When the contact angle further reduces to $\theta_{c,\ HTW}$ (red line in Fig. 14), the HTWs completely vanish and only the irregular oscillatory BM convection remains in the droplet. With decreasing the Ma number, both the critical contact angles ($\theta_{c,OBM}$) for the onset

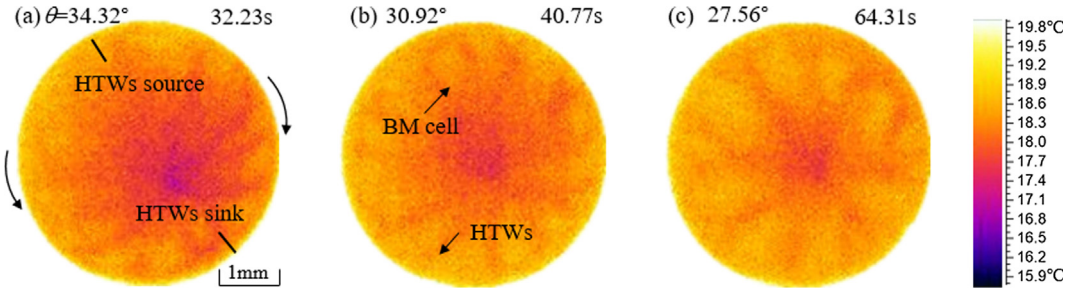

Fig. 13. Evolution of the surface temperature patterns of a droplet with the radius of $R = 2.12$ mm at $T_w = 18.79$ °C, $T_a = 21.03$ °C and the relative humidity of 51% for (a) $\theta = 34.23°$ at $t = 32.23$ s, (b) $\theta = 30.92°$ at $t = 40.77$ s and (c) $\theta = 27.56°$ at $t = 64.31$ s.

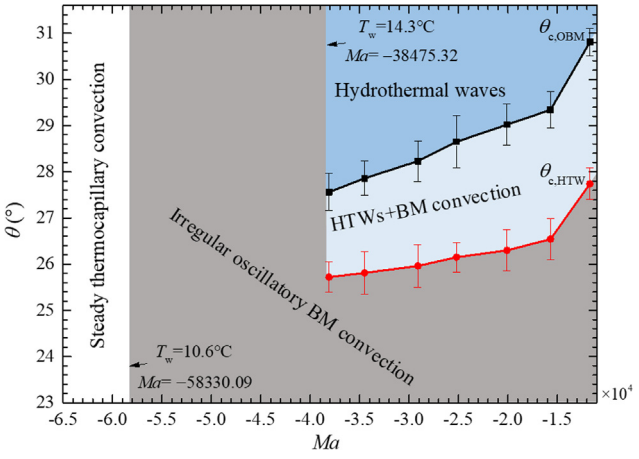

Fig. 14. The critical contact angle for incipience of Marangoni convection instabilities for $T_w < T_a$. The error bar indicates the discrepancy between the maximum value of contact angle from the average one.

of the irregular oscillatory BM convection and those ($\theta_{c,HTW}$) for the disappearance of HTWs decrease. As mentioned above, with decreasing the T_w, the normal temperature gradient becomes smaller and it makes BM cells appear more difficultly. The BM cells can only occur with a relative smaller contact angle because only on this occasion the Marangoni force perpendicular to the droplet surface is big enough to make BM convection lose its instability. Thus the critical contact angle ($\theta_{c,OBM}$) for the onset of irregular oscillatory BM convection decreases with decreasing *Ma* number, and for the same reason, $\theta_{c,HTW}$ also decreases with decreasing *Ma* number. For $-58330.09 \le Ma \le -38475.32$ ($10.6\ °C \le T_w \le 14.3\ °C$), only the irregular oscillatory BM convection occurs.

It is well known that the BM convection can only occur and sustain in a flat liquid layer subjected to a negative temperature gradient, i.e., the bottom temperature is higher than that of the top surface. However, present results show that the BM patterns occur in a droplet even when the bottom temperature is lower than its surface temperature. For example, the temperature difference between the bottom and the apex is $\Delta T^* = -0.43$ °C when $T_w = 12.45$ °C shown in Fig. 10(a) which is measured by the thermocouples with diameter of 0.025 mm (Omega Engineering Inc.). The similar phenomenon was observed in a 1-mm-thick alcohol layer cooled from below by Zhang and Chao [35] and they considered that the evaporation plays an important role in such case and a modified *Ma* number (Ma^*) included in the evaporating cooling effect was proposed to explain such phenomenon, which is written as

$$Ma^* = \frac{|\gamma_T|\Delta T^* H}{\mu a} + \frac{|\gamma_T| V' \Delta h_v H^2}{\mu c_p a^2}$$

where Δh_v is the latent heat of vaporization and V' is the volumetric evaporation rate per unit area. The first item is the traditional *Ma* number which represents the effect of temperature difference and the second item represents the influence of the evaporation. By this definition, the Ma^* equals to be 268.11 with $V' = 6.58 \times 10^{-7}$ m/s in Fig. 10(a). Here, the V' is the volumetric evaporation rate per unit average surface area of the droplet and the volumetric evaporation rate is measured according to the droplet deformation through the contact angle measurement. According to the explanation of Zhang and Chao [35], the vapor recoil is another important reason that reduces to the BM convection. Liu et al. [36] found that the vapor recoil can destabilize the stability of the BM convection. That is why the BM convection occurs even under positive temperature gradient.

4. Conclusions

A series of experiments are conducted to investigate the Marangoni convection instabilities in a sessile droplet evaporating at CCL mode in a wide range of substrate temperature from lower than room temperature to that higher than room temperature. The BM convection cells are observed for $T_w > T_a$. With evaporation, the cell patterns vary from the quasi-steady state to irregular oscillatory state. The maximum cell number of the quasi-steady BM patterns increases with the increase of substrate temperature. The critical contact angles for the onset of steady BM convection and those for the onset of irregular oscillatory BM convection increase with the increase of substrate temperature.

For $T_w < T_a$, the irregular oscillatory BM cells are observed when T_w higher than 10.6 °C. The cell size is larger while the cell number is smaller than that for $T_w > T_a$. The cells are very weak. When T_w is higher than 14.3 °C the travelling hydrothermal waves, coexistence of the HTWs and the irregular oscillatory BM convection, and the irregular oscillatory BM convection occurs successively with droplet evaporating. The critical contact angles for the onset of the irregular oscillatory BM convection and those for the disappearance of the HTWs decrease with the decreasing of substrate temperature.

Conflict of interest

The authors declared that there is no conflict of interest.

Acknowledgement

This work was funded by the National Nature Science Foundation of China (Nos. 51676018 and 51176210).

References

[1] C. Edwards, A. Arbabi, B. Bhaduri, X. Wang, R. Ganti, P.J. Yunker, A.G. Yodh, G. Popescu, L.L. Goddard, Measuring the nonuniform evaporation dynamics of sprayed sessile microdroplets with quantitative phase imaging, Langmuir 31 (2015) 11020–11032.

[2] M.S. Ren, J. Sweelssen, N. Grossiord, H. Gorter, T.M. Eggenhuisen, R. Andriessen, Inkjet printing technology for OPV applications, J. Imag. Sci. Technol. 56 (2012) 040504.

[3] V. Dugas, J. Broutin, E. Souteyrand, Droplet evaporation study applied to DNA chip manufacturing, Langmuir 21 (2005) 9130–9136.

[4] S.T. Chang, O.D. Velev, Evaporation-induced particle microseparations inside droplets floating on a chip, Langmuir 22 (2006) 1459–1468.

[5] H. Hu, R.G. Larson, Analysis of the effects of Marangoni stresses on the microflow in an evaporating sessile droplet, Langmuir 21 (2005) 3972–3980.

[6] K. Sefiane, J.R. Moffat, O.K. Matar, R.V. Craster, Self-excited hydrothermal waves in evaporating sessile drops, Appl. Phys. Lett. 93 (2008) 074103.

[7] G. Karapetsas, O.K. Matar, P. Valluri, K. Sefiane, Convective rolls and hydrothermal waves in evaporating sessile drops, Langmuir 28 (2012) 11433–11439.

[8] K. Sefiane, A. Steinchen, R. Moffat, On hydrothermal waves observed during evaporation of sessile droplets, Colloids Surf. A Physicochem. Eng. Asp. 365 (2010) 95–108.

[9] K. Sefiane, Y. Fukatani, Y. Takata, J. Kim, Thermal patterns and hydrothermal waves (HTWs) in volatile drops, Langmuir 29 (2013) 9750–9760.

[10] B. Sobac, D. Brutin, Thermocapillary instabilities in an evaporating drop deposited onto a heated substrate, Phys. Fluids 24 (2012) 032103.

[11] F. Carle, B. Sobac, D. Brutin, Hydrothermal waves on ethanol droplets evaporating under terrestrial and reduced gravity levels, J. Fluid Mech. 712 (2012) 614–623.

[12] X. Zhong, F. Duan, Stable hydrothermal waves at steady state evaporating droplet surface, Sci. Rep. 7 (2017) 16219.

[13] H. Bénard, Swirling movements of cellular structure. Optic study of free surfaces, Comptes Rendus Hebdomadaires Des Seances De L Academie Des Sciences 130 (1900) 1065–1068.

[14] H. Bénard, Experimental studies on the movement of liquids propagated by heat by means of convection. Permanent system: cellular turbulence, CR Hebd. Seances Acad. Sci. 130 (1900) 1004–1007.

[15] M.J. Block, Surface tension as the cause of Bénard cells and surface deformation in a liquid film, Nature. 4534 (1956) 650–651.

[16] J.R.A. Pearson, On convection cells induced by surface tension, J. Fluid Mech. 4 (1958) 489–500.

[17] S.J. VanHook, M.F. Schatz, W.D. McCormick, J.B. Swift, H.L. Swinney, Long-wavelength instability in surface-tension-driven Bénard convection, Phys. Rev. Lett. 75 (1995) 4397–4400.

[18] H. Mancini, D. Maza, Pattern formation without heating in an evaporative convection experiment, Europhys. Lett. 66 (2004) 812–818.

[19] E.L. Koschmieder, M.I. Biggerstaff, Onset of surface-tension-driven Bénard convection, J. Fluid Mech. 167 (1986) 49–64.

[20] M.F. Schatz, S.J. Vanhook, W.D. Mccormick, J.B. Swift, H.L. Swinney, Time-independent square patterns in surface-tension-driven Bénard convection, Phys. Fluids. 11 (1999) 2577–2582.

[21] M.F. Schatz, S.J. Vanhook, W.D. Mccormick, J.B. Swift, H.L. Swinney, Onset of surface-tension-driven Bénard convection, Phys. Rev. Lett. 75 (1995) 1938–1941.

[22] K. Nitschke, A. Thess, Secondary instability in surface-tension-driven Bénard convection, Phys. Rev. E 52 (1995) 5772–5775.

[23] M. Bestehorn, Square patterns in Bénard-Marangoni convection, Phys. Rev. Lett. 76 (1996) 46–49.

[24] N.L. Zhang, W.J. Yang, Microstructure of flow inside minute drops evaporating on a surface, J. Heat Transfer 105 (1983) 908–910.

[25] W.Y. Shi, K.Y. Tang, J.N. Ma, Y.W. Jia, H.M. Li, L. Feng, Marangoni convection instability in a sessile droplet with low volatility on heated substrate, Int. J. Therm. Sci. 117 (2017) 274–286.

[26] S. Semenov, F. Carle, M. Medale, D. Brutin, 3D unsteady computations of evaporative instabilities in a sessile drop of ethanol on a heated substrate, Appl. Phys. Lett. 111 (2017) 241602.

[27] S. Semenov, F. Carle, M. Medale, D. Brutin, Boundary conditions for a one-sided numerical model of evaporative instabilities in sessile drops of ethanol on heated substrates, Phys. Rev. E. 96 (2017) 063113.

[28] J.L. Zhu, W.Y. Shi, L. Feng, Bénard-Marangoni instability in sessile droplet evaporating at constant contact angle mode on heated substrate. Under review.

[29] A.D. Pline, Infrared surface temperature measurements for the surface tension driven convection experiment, NASA Tech. Memo. 101353 (1989) 1–23.

[30] N.A. Ospennikov, D. Schwabe, Thermocapillary flow without return flow-linear flow, Exp. Fluids 36 (2004) 938–945.

[31] H. Mancini, D. Mana, Pattern formation without heating in an evaporative convection experiment, Europhys. Lett. 66 (2004) 812–818.

[32] A.I. Mizev, D. Schwabe, Convective instabilities in liquid layers with free upper surface under the action of an inclined temperature gradient, Phys. Fluids 21 (2009) 112102.

[33] S.J. Vanhook, M.F. Schatz, W.D. Mccormick, J.B. Swift, H.L. Swinney, Long-wavelength instability in surface-tension-driven Benard convection, Phys. Rev. Let. 75 (1995) 4397–4400.

[34] O.E. Shklyaev, A.A. Nepomnyashchy, Thermocapillary flows under an inclined temperature gradient, J. Fluid Mech. 504 (2004) 99–132.

[35] N.L. Zhang, D.F. Chao, Mechanisms of convection instability in thin liquid layers induced by evaporation, Int. Commun. Heat Mass 26 (1999) 1069–1080.

[36] R. Liu, Q.S. Liu, Vapour recoil effect on a vapour-liquid system with a deformable interface, Chin. Phys. Lett. 23 (2006) 879–882.